Mechanistic Studies on the Base-Catalyzed Transformation of Neocarzinostatin Chromophore: Roles of Bulged DNA†

Zhen Xi, Qun Kai Mao, and Irving H. Goldberg*

Department of Biological Chemistry and Molecular Pharmacology, Harvard Medical School, Boston, Massachusetts 02115

Received November 17, 1998; Revised Manuscript Received February 3, 1999

ABSTRACT: Nucleic acid bulges have been implicated in a number of biological processes and are specific cleavage targets for the enediyne antitumor antibiotic neocarzinostatin chromophore (NCS-chrom) in a base-catalyzed, radical-mediated reaction. Studies designed to elucidate the detailed mechanism of the base-catalyzed activation of NCS-chrom and to evaluate the roles of bulged DNA in its activation are described. They show that nucleobases in the DNA bulge are not required to form an effective bulge pocket but enhance the binding of the wedge-shaped activated drug molecule. Analysis of solvent deuterium isotope effects on NCS-chrom degradation and DNA cleavage efficiency experiments suggests that the spirolactone biradical **6** is a relatively stable species and that intramolecular quenching of the C2 radical of **6** to form the biologically active cyclospirolactone radical **7a** occurs first (pathway a in Scheme 2), leaving the C6 radical to abstract the hydrogen atom from the DNA deoxyribose and to form the cyclospirolactone **8**. Binding of the activated drug at the bulge site is required, but not sufficient, for efficient **8** formation, whereas cleavage of bulged DNA is not essential. Efficient generation of **8**, but inefficient DNA damage generation, comes mainly from the likely high off-rate of **7a** binding. The finding that thymidine 5′-carboxylic acid-ended oligonucleotide fragment can be formed in the reaction suggests that the process of DNA cleavage is rather slow and that sequential oxidations of the target 5′-carbon are possible. Study of the effect of solvent (methanol) concentration on NCS-chrom degradation indicates that bulged DNA acts to assist the intramolecular quenching of the radical at C2 by C8″ of the naphthoate moiety by excluding solvent from the binding pocket, thus preventing the formation of spirolactones **9**, and by blocking radical polymerization. Because in the absence or near absence of solvent methanol **8** formation does not reach even 10% that formed in the presence of bulged DNA, it is possible that the DNA bulge also induces a conformational change in the drug to promote the intramolecular reaction.

Neocarzinostatin (NCS) belongs not only to a superfamily of antibiotics containing enediyne structures but also to a superfamily of macromolecular protein antibiotics (*1* and references therein). It was only after it was appreciated that the active component of the macromolecular complex was a small nonprotein chromophore that it was possible to begin to understand its interaction with DNA in molecular terms. These studies, in conjunction with those on the related agents calicheamicin/esperamicin, have uncovered novel mechanisms of DNA damage, wherein a biradical species of the active drug acts as a sequence-selective, bistrand-reactive agent through hydrogen abstraction from the sugar residues of DNA.

The thiol-dependent activation of NCS-chrom **1** (Scheme 1), the biologically active chromophoric component of NCS, involves nucleophilic attack by thiol at C12 in trans configuration (*2*) to the naphthoate at C11 and epoxide opening at C5 to generate the nine-membered ring enyne-cumulene **2**, which cyclizes between C3 and C7 to form a 2,6-didehydroindacene biradical **3** (*3*, *4*). The biradical abstracts hydrogen atoms from sources such as solvent and/or DNA deoxyribose moiety to give a postactivated tetrahydroindacene reduction product **4** (*4*, *5*). An NMR-derived solution structure of the thiol-postactivation product **4**, which is isostructural with the active biradical form **3** of the drug, and duplex DNA, in which the naphthoate acts as an intercalating moiety and the didehydroindacene biradical lies

Scheme 1: Proposed Mechanism for the Thiol Activation of NCS-chrom

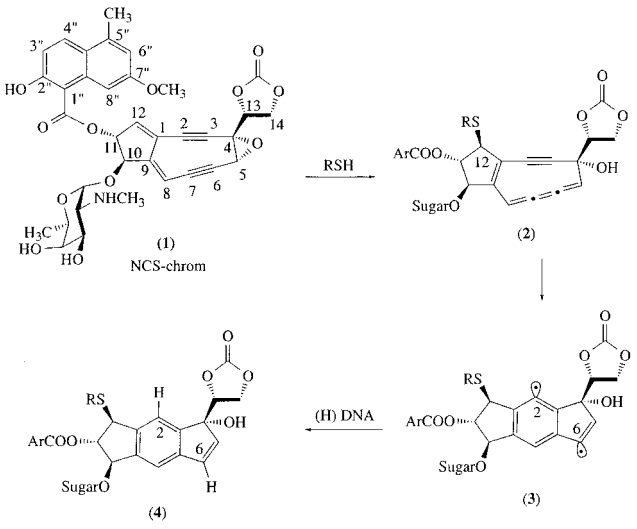

† This work was supported by U. S. Public Health Service Grant GM53793 from the National Institutes of Health.

* To whom correspondence should be addressed.

10.1021/bi982734i CCC: $18.00
Published on Web 03/19/1999

Scheme 2: Proposed Mechanistic Pathways of Based-Catalyzed Activation of NCS-chrom

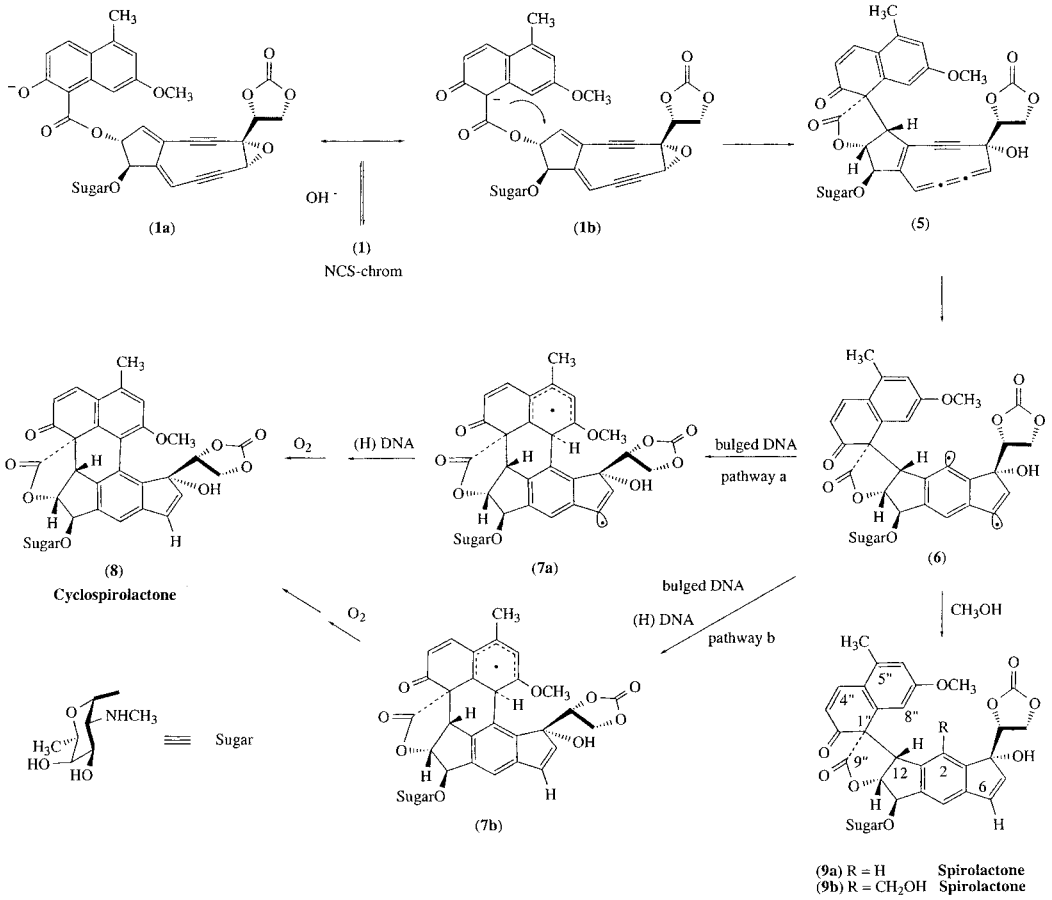

in the DNA minor groove, has clarified the mechanism of sequence-specific DNA sugar damage (*6*).

In 1993 it was observed that an oligodeoxynucleotide containing a two-base bulge can be highly efficiently and specifically cleaved by NCS-chrom **1** at the bulge site in the absence of thiol at pH ≥ 6 (*7*, *8*). Cleavage was restricted to a target nucleotide at the 3′ side of the bulged DNA and was entirely due to 5′-chemistry, with the formation of oligonucleotide fragments with 3′-phosphate and 5′-nucleoside 5′-aldehyde ends. Later, it was found that HIV TAR RNA can also be cleaved in a similar fashion, albeit much less efficiently (*9*). On the basis of the determination of the structures of the postactivated NCS-chrom drug products in the presence and absence of bulged DNA, a base-catalyzed intramolecular activation mechanism of NCS-chrom **1** was proposed, as shown in Scheme 2 (*10*, *11*).

In this mechanism, the spirolactone cumulene **5** is generated stereospecifically via a general base-catalyzed intramolecular Michael addition at C12 by the enolate anion **1b**, which is a resonance form of the naphtholate anion **1a** of NCS-chrom **1**, resulting in the formation of the 2,6-didehydroindacene biradical **6**. This cascade of reactions occurs spontaneously, and in the absence of bulged DNA the biradical is quenched by other hydrogen sources, such as methanol in the solvent, to yield spirolactones **9**. It is of particular interest that the cyclospirolactone **8** is generated virtually only in the presence of substrate-bulged DNA and is the only drug product to contain ^{3}H abstracted from the 5′ position of the targeted bulge nucleotide. Thus, it has been proposed that in the presence of bulged DNA, the spirolactone cumulene **5**, which has been implicated as the binding species that searches for the favored DNA binding site, is in equilibrium between bound and free forms, which leads to cyclospirolactone **8** and to spirolactones **9**, respectively, via spirolactone biradical **6**.

The base-catalyzed activation of NCS-chrom **1** to a biradical species, capable of selectively and specifically cleaving DNA at a bulged site and generating bulge-specific drug product cyclospirolactone **8**, has raised a number of interesting mechanistic questions, among them, the possible role(s) of the DNA in effecting formation of **8**. In the absence of substrate-bulged DNA, spirolactones **9a** and **9b** are formed spontaneously and **8** is barely detectable. A recent NMR solution structure of the complex formed between **9a**, the analogue of the putative cleaving species indacene biradical **6**, and a two-base bulged oligodeoxynucleotide showed that the wedge-shaped **9a**, with its planar naphthoate and indacene ring systems held rigidly at a 60° angle to each other by the connecting spirolactone, fits snugly in the triangular prism bulge binding pocket, formed by the two looped-out bulge bases and the neighboring base pairs (*12*). The radical center at C6 is thus strategically placed only 2.2 Å from the *pro-S* H5′ of the targeted bulge nucleotide. Does the bulged DNA, then, act to assist the intramolecular quenching of the radical at C2 by C8″ of the naphthoate moiety solely by excluding solvent (methanol, solvent for the drug) from the tight binding pocket, or does it also induce a conformational change in the drug to promote the reaction? Also, what is the requirement for an effective bulge capable of generating cyclospirolactone **8**? Further, does the intramolecular quench-

ing of the radical at C2 precede hydrogen abstraction from the DNA deoxyribose (pathway a), or does it occur concurrently with the abstraction (pathway b). Experiments designed to address these questions are presented here.

MATERIALS AND METHODS

Materials. Nucleoside phosphoramidites, chemical linkers, poly-pak cartridges for purification of trityl-on oligonucleotides, as well solvents and reagents for DNA synthesis, were from Glen Research. T4 polynucleotide kinase and Klenow fragment of DNA polymerase I were from New England Biolabs. S1 nuclease and calf intestinal alkaline phosphatase were from Boehringer Mannheim. Snake venom phosphodiesterase and bacterial alkaline phosphatase were from Pharmacia Biotech. [γ-^{32}P]Adenosine triphosphate and [α-^{32}P]-guanosine triphosphate were from New England Nuclear Dupont. Deuterated solvents were from Cambridge Isotope Laboratories. All other chemicals were from either Sigma or Aldrich.

Synthesis of Oligonucleotides. Oligonucleotides (Figure 1) were synthesized using standard β-cyanoethyl phosphoramidite methodology on an ABI 381A DNA synthesizer. The trityl-on procedure was used in most cases. The synthesized oligonucleotides were deprotected in 30% ammonium hydroxide at 55 °C for 15 h and purified using poly-pak cartridges. The purity of oligonucleotides was verified by either HPLC or sequencing gel electrophoresis. Concentrations of oligomers were determined using the additive extinction coefficiency method, with only nucleobases being counted (*13*).

^{32}P End-Labeling of Oligonucleotides. Oligonucleotides were 5′- ^{32}P end-labeled with [γ-^{32}P]ATP and T4 polynucleotide kinase. 3′- ^{32}P-labeled oligomers were prepared using the fill-in method with [α-^{32}P]GTP and Klenow fragment of DNA polymerase I. The ^{32}P-labeled oligomers were purified by electrophoresis on a 15% sequencing gel. The appropriate bands were exercised, crushed and soaked, and desalted with the use of G-25 Sephadex columns (*14*).

NCS-chrom Reaction. Neocarzinostatin powder was obtained from Kayaku Antibiotics (Tokyo). NCS-chrom was extracted from lyophilized holo-NCS dry powder with 0.5 M acetic acid in methanol in the dark (*15*). The extracts were evaporated under vacuum at below −15 °C. The yellowish, light-sensitive pellet was redissolved in cold methanol or other solvents such as tetrahydrofuran, acetonitrile, or ethanol, as needed. The extracts were stored at −80 °C in the dark. The upper clear solution of the extract was used as drug stock. The concentration of NCS-chrom stock was determined with apo-NCS at a wavelength of 340 nm (ϵ = 10 800) (*16*).

The 5′- or 3′-^{32}P-labeled oligonucleotides were annealed to their complementary strands (typically 1:2 ratio) in 2× reaction buffer by heating at 90 °C for 3 min and slowly cooling back to room temperature. Adjustment of the final reaction volume was made by addition of water (*17*). A typical drug/DNA reaction was carried out in a volume of 40 μL containing 50 mM Tris·HCl (pH 8.5), 1 mM EDTA, 10% methanol, and appropriate concentrations of drug and oligonucleotides, as indicated. In some reactions, EDTA was omitted, which was found to give the same experimental outcome as that with EDTA. The reaction mixture was

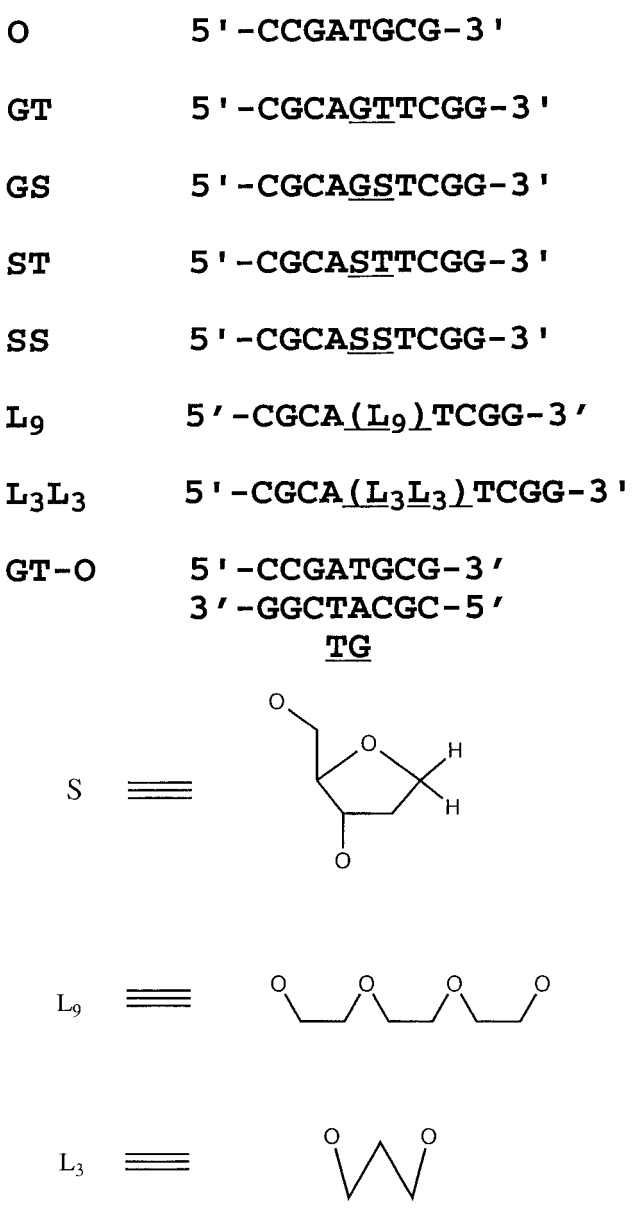

FIGURE 1: Sequences of oligonucleotides. GT-O = annealed duplex of oligomers GT and O in a ratio of 1:2; same holds true for GS-O, ST-O, SS-O, L_3L_3-O and L_9-O. Underlining indicates bulged nucleotides or linker in the duplex.

chilled on ice for 15 min prior to the addition of NCS-chrom. The incubation proceeded on ice in the dark for 1−5 h, as indicated. An aliquot of the reaction mixture was either speed-vac dried, resuspended in 80% formamide sequencing loading buffer prior to electrophoresis, or frozen in liquid nitrogen prior to HPLC analysis.

Postreaction Treatment. Alkaline treatment of the sample was carried out by heating one of the duplicate aliquots in 50 μL of 1 M piperidine (PIP) at 90 °C for 30 min. The piperidine was removed by coevaporation with water three times using speed-vac. Hydrazine treatment (HZ) was carried out in 100 mM hydrazine (pH 8.0) at room temperature for 1 h. $NaBH_4$ treatment was carried out in 0.2 M $NaBH_4$ for 2 h. Borane hydride treatment was carried out in 80 mM BH_3/pyridine aqueous solution by addition of 1 M BH_3/pyridine complex in 2-propanol, and the cocktail was incubated at room temperature for 20 h (*18*). Sodium

hypoiodite (NaOI) treatment of the 5′-aldehyde reaction product was carried out in 15 mM NaOI by addition of the mixture of 0.1 M KI_3 and 0.5 M Na_2CO_3 (pH 9.0). The cocktail was incubated at room temperature for 30 min, neutralized with cold 1 N HCl, and treated with 15 mM $Na_2S_2O_3$ to get rid of excess oxidizing agent before drying (*19*).

Alkaline phosphatase treatment involved incubation of calf intestinal phosphatase with substrate at 37 °C for 1 h. Enzyme digestion of oligonucleotides into nucleosides was accomplished with a mixture of bacterial alkaline phosphatase and snake venom phosphodiesterase.

Polyacrylamide Gel Electrophoresis Analysis. Fifteen percent denaturing polyacrylamide gels were prepared using Sequagel stock from National Diagnostics. Electrophoresis was performed in a 1× TBE buffer at room temperature and 1000−1500 V. The gel bands were quantitated with a Molecular Dynamics PhosphorImager by performing volume integration using Image Quant 3.4. The bands of interest were sometimes excised from the gel. The crush and soak method was used with water at 4 °C overnight. The eluent was desalted through G-25 Sephadex columns or Sep-pak columns and speed-vac dried or lyophilized for further use.

Fluorescence Studies. Fluorescence measurements were carried out on a Perkin-Elmer LS50B luminescence spectrometer. A typical measurement consisted of 1−2 μM of drug in 50 mM Tris·HCl buffer at 4 °C. Concentrations of DNA and methanol and pH were varied as indicated. The excitation was at 400 nm, and emission spectra were recorded from 420 to 600 nm. The emission at 550 nm was used in the calculation of initial rate constants (*20*).

The rates of NCS-chrom degradation with or without oligonucleotides were measured using the time-drive method on the fluorescence spectrometer. The plot of $\ln(100 - F_t)$ vs time was a linear fit to the equation:

$$\ln(100 - F_t) = \ln(100 - F_0) - kt$$

where F_t is the fluorescence at incubation time t and F_0 is the fluorescence value at $t = 0$. The initial rate constant for the pseudo first order of NCS-chrom disappearance was equal to the slope of the line.

HPLC Analysis. A linear gradient consisting of mobile phase A and B with flow rate 1 mL/min was applied to a reverse phase C18 column (Rainin Microsorb-MV C18). Elution was monitored by following UV absorbance (254 or 340 nm) and fluorescence (ex 400 nm, em 550 nm). Different sets of mobile phase A and B were used. Set A consisted of 5 mM aqueous ammonium acetate (pH 4.0) (mobile phase A) and 5 mM methanolic ammonium acetate (mobile phase B). Set B was composed of 100 mM aqueous triethylamine acetate (pH 7.0) (mobile phase A) and acetonitrile (mobile phase B). Quantitation was carried out by area integration of fluorescence and UV peaks of interest. Calibration experiments were based on the integrated areas of HPLC peaks to the molar equivalency of the drug. The experimental results were in the linear range.

Isolation, Purification, and Identification of Thymidine 5′-Carboxylic Acid-Ended Fragment. Thymidine 5′-carboxylic acid-ended fragment was isolated by sequencing gel electrophoresis. Reactions contained 50 mM Tris·HCl (pH 8.5), 2 μM 3′-^{32}P-labeled oligonucleotide GT of GT-O (Figure 1) and 150 μM NCS-chrom. The gel bands corresponding to thymidine 5′-carboxylic acid-ended fragment (CA) were excised, crushed and soaked with water. The extracts were purified by reverse phase HPLC. The purified CA band was analyzed by (1) postreaction treatment as shown in Figure 10, (2) HPLC analysis of the enzyme digest, which gave rise to an abnormal nucleoside peak comigrating with authentic sample of thymidine 5′-carboxylic acid, and (3) by mass spectrometry.

Mass Measurement. Mass measurement was carried out with Perseptive Biosystem's Voyager-DE biospectrometry workstation, using delayed extraction matrix-assisted laser desorption ionization time-of-flight (MALDI-TOF) mass analysis.

RESULTS AND DISCUSSION

Solvent Effect on Base-Catalyzed Transformation of Neocarzinostatin Chromophore. It is striking that cyclospirolactone **8** is the predominant drug metabolite (>90% yield) in the presence of excess bulged DNA (Figure 2). Variation of the methanol concentration gave rise to different yields of cyclospirolactone **8** (always <10%) in the case of degradation of NCS-chrom without bulged DNA, but yielded the same amount of **8** with excess bulged DNA. When degradation of NCS-chrom was carried out in 12.5 M methanol, spirolactones **9** were isolated with over 90% yield, with **9a** over 80% (the identities of **8** and **9** were confirmed by mass measurement). As shown in Scheme 2, there are two different possible pathways for the quenching of the C2 radical center in 2,6-didehydroindacene biradical **6**, which lead to two different types of products **8** and **9**; the actual pathway will be the result of combined kinetic and thermodynamic control.

A biradical, such as **6**, is a relatively reactive species with a short half-life, even if much less reactive than a monoradical, such as the alkenyl and phenyl radical (*21*−*25*). Because quenching of the radical at C2 is unimolecular in the formation of cyclospirolactone **8**, whereas it is bimolecular in **9** formation involving solvent methanol at C2, the easiest way to alter the fate of biradical **6** is through manipulation of the concentration of the hydrogen source, i.e., the solvent. Two practical approaches have been chosen: (i) controlling the concentration of radical quenching sources, such as abstractable hydrogen sources; (ii) high dilution to avoid radical-based polymerization (*26*).

A systematic study of the solvent concentration effect shows that methanol inhibits the formation of the drug metabolite **8** (Figures 2 and 3); the yield of **8** rises steeply at the lowest concentrations of methanol to a maximum of only about 8% of that generated in the presence of substrate-bulged DNA (Figure 3, inset). Similar results were observed with other hydrogen sources, such as acetonitrile and tetrahydrofuran. At very low concentrations of methanol, **8** becomes the major product and **9a** and **9b** reach almost negligible amounts, confirming the elimination of active external hydrogen sources. Noncharacterizable UV absorption eluting at 100% methanol on HPLC and found only at <0.5 M methanol was tentatively assigned to polymeric material resulting from radical-based polymerization. These combined results suggest that bulged DNA enhances formation of **8** not only by excluding hydrogen sources (organic solvent) from the binding pocket but by preventing radicals

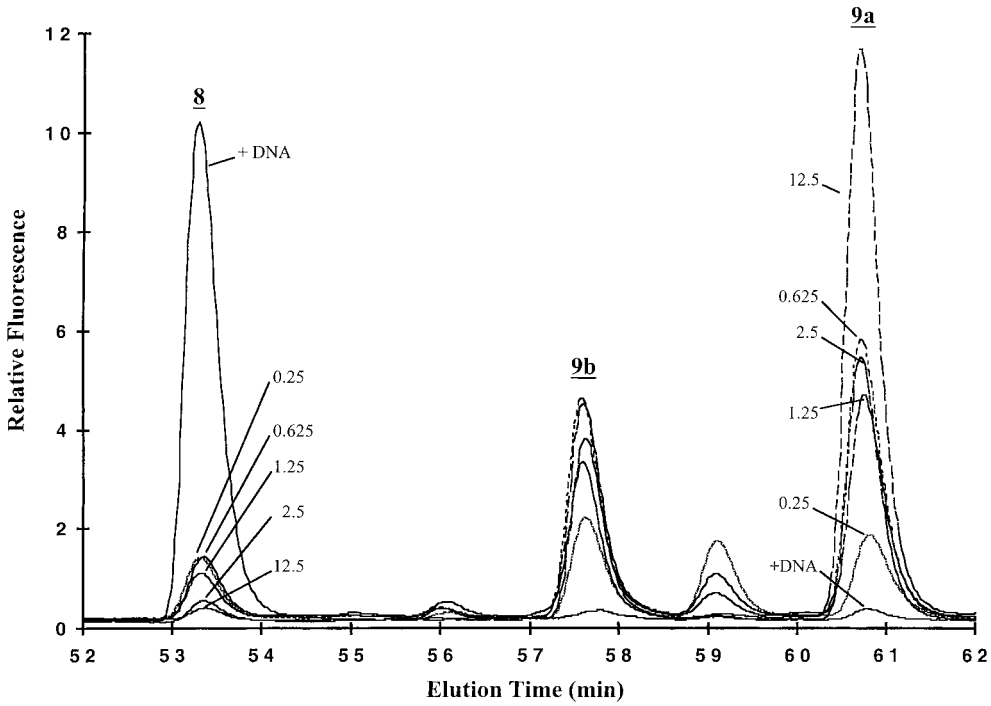

FIGURE 2: HPLC profile of the degradation products of NCS-chrom under basic conditions with or without bulged DNA. The labels (0.25, 0.625, 1.25, 2.5, and 12.5) of HPLC peaks for **8**, **9a**, and **9b** refer to the molar concentration of methanol. +DNA refers to the reaction in the presence of 4-fold excess bulged GT of GT-O to NCS-chrom. The peak at elution time 59.2 min has not been structurally characterized. NCS-chrom (5 μM) was incubated in phosphate buffer (25 mM, pH 7.6) at 4 °C for 1 h in the presence of varying concentrations of methanol (0−12.5 M). Reverse phase HPLC on a C18 column (linear gradient of 0−100% methanol in 5 mM ammonium acetate, pH 4.0) was used to quantitate the formation of drug metabolites. Elution was monitored by following 254 nm UV absorbance and 550 nm fluorescence (excitation at 400 nm).

from reacting with each other. Further, when NCS-chrom was diluted from 5 μM to 0.5 μM, the yield of **8** did not increase (data not shown), implying that its formation, through intramolecular radical addition to form the C2−C8″ bond, is not an efficient process. The experimentally found monotonic inhibition curve for **8** formation also suggests that C2−C8″ bond formation is not efficient. If C2−C8″ bond formation were more efficient than polymerization, the concentration profile of methanol should yield a bell-shaped curve; at very low concentrations of methanol, polymerization will prevail, while at increasing concentrations, a point, at which the methanol concentration is not high enough for the efficient formation of **9**, will be reached where C2−C8″ bond formation (intramolecular radical cyclization) peaks. These experiments indicate that bulged DNA assists C2−C8″ bond formation by protecting the C2 radical of **6** from access by solvent sources of hydrogen, as well as by other radical molecules. These actions, however, increase the yield of **8** to a maximum of less than 10% of the yield found with substrate-bulged DNA, leaving open the possibility that bulged DNA also induces a conformational change in **6** (thus lowering its transition state energy) to favor formation of the cyclospirolactone **8**.

It is especially interesting to note that spirolactone **9b** with a hydroxymethyl group bonded to the C2, but not the C6 position, is the only product containing the hydroxymethyl group generated in the presence of methanol. This is remarkable considering the very reactive nature of radicals. It is reasonable to assume that spirolactone **9b** comes from a bound form of the hydroxymethyl radical, generated by the drug radical abstracting hydrogen from a methanol molecule, because a free form of such a radical would certainly be expected to yield a mixture, probably with bond formation at C6 being favored. The bound form of the hydroxymethyl radical is likely generated from either a bound form of the methanol molecule or from a caged radical. Either way, this calls for the participation of the naphthoate group in complex formation. It is intriguing to speculate that a methanol molecule preferentially interacts with the planar naphthoate group through either σ, π interaction or hydrogen bonding through the 7″-methoxy group. The latter is less likely as the fucosamine residue close to the C6 position may also have hydrogen bonding ability to direct the hydroxymethyl radical to the C6 position. The fact that the production of spirolactone **9b** approached a plateau as the concentration of methanol increased to 2 M (Figure 3) supports the possibility that the methanol molecule binds preferentially to the planar naphthoate group. The binding is weak, but site-specific, and reaches saturation at a certain concentration of methanol. This may represent a rare instance where a methanol molecule interacts with an aromatic system through σ, π interaction.

Solvent Isotope Effect on NCS-chrom Degradation. When base-catalyzed activation of NCS-chrom was carried out using deuterated methanol (methanol-d4, D > 99.99%) in the absence of substrate-bulged DNA, a solvent isotope effect was observed for the formation of cyclospirolactone **8** and spirolactones **9** (Figure 4). Formation of spirolactone **9a** was dramatically influenced by using deuterated methanol; the solvent isotope effect (k_H/k_D) ranges from 18 to 4.9 depending on the methanol concentration. As for the formation of spirolactone **9b**, the solvent isotope effect (k_H/k_D) ranges from 2.3 to 1.2. The inverse solvent isotope effect (k_H/k_D) for formation of cyclospirolactone **8** ranges from 1.8 to 4.1.

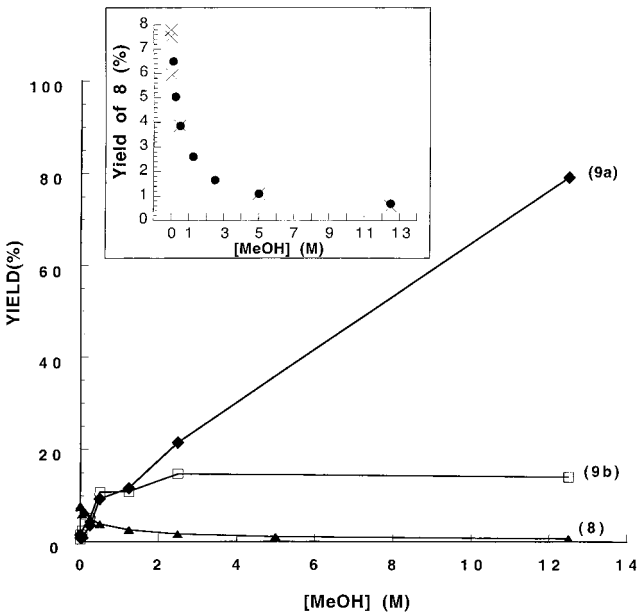

FIGURE 3: Influence of methanol concentration on degradation of NCS-chrom. Inset shows the yield of **8** at the lowest concentrations of methanol. (×) represents a set of experiments carried out with solvent-free NCS-chrom (vide infra); (●) represents a set of experiments carried out with NCS-chrom not made solvent-free before use. Solvent-free NCS-chrom was obtained by drying a solution of the drug in methanol (0.1 M acetic acid) at high vacuum in glass tubes at −40 °C immediately before use. The amount of active NCS-chrom in the preparation was assessed by incubation in the presence of an excess (4 molecular equiv) of substrate-bulged DNA (GT-O) and determination of the yield of **8**; the latter was found to be the only drug species (>95%) detectable by either UV or fluorescence, whether the drug was incubated in 5M methanol or was solvent-free. Reaction conditions and HPLC analysis were as in Figure 2. Quantitation was based on integration of UV absorbance.

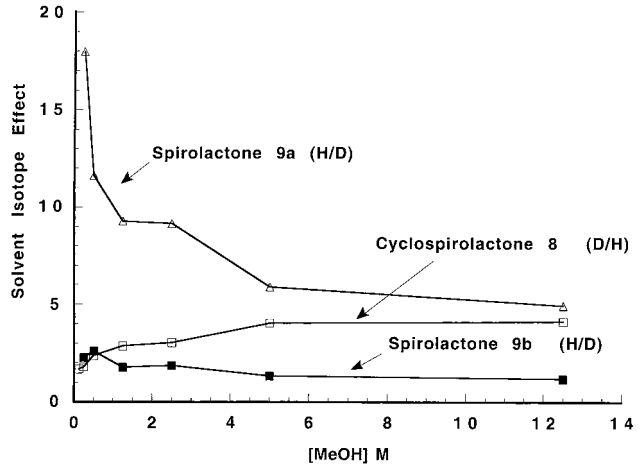

FIGURE 4: Influence of deuterated methanol on product distribution of NCS-chrom degradation compared with protium methanol. Drug products were quantitated by HPLC analysis, as in Figure 2. NCS-chrom (5 μM) was incubated in phosphate buffer (25 mM, pH 7.6) at 4 °C for 1 h in the presence of varying concentrations of methanol (0.25−12.5 M). In the deuterated experiment, deuterated methanol (MeOH-d4, D > 99.99%) was also used for extraction of NCS-chrom from holo-NCS. Note that solvent isotope effects are expressed as H/D for spirolactones **9a** and **9b** and D/H for cyclospirolactone **8** for convenience.

These results are summarized in Table 1. The strong solvent isotope effect for **9a** formation (k_H/k_D = 4.9) at 12.5 M methanol, where **9a** is the major product, shows that hydrogen abstraction (by C2, vide infra) is the rate-determining process and that the biradical is a relatively stable species. The solvent isotope effect (k_H/k_D) for **9b** formation approaches 1 as the methanol concentration increases, i.e., no significant solvent isotope effect for the formation of **9b**. The formation of **9b** presumably involves hydrogen abstraction by both C2 and C6 radical centers of biradical **6** and subsequent hydroxymethyl radical addition to the C2 position. Therefore, a solvent isotope effect of 1 indicates that hydrogen abstraction at neither radical center is rate-limiting, suggesting that the intramolecular-like (vide supra) hydroxymethyl radical addition to C2 is the rate-determining step. Because it is unlikely that the latter step is slower than the intermolecular biradical hydrogen abstraction by C6, it appears that hydrogen abstraction by the C2 radical, not the C6 radical, occurs first. Consistent with this formulation, it would be reasonable for the intramolecular-like hydrogen abstraction by the C2 radical to be faster than the intramolecular-like hydroxymethyl radical addition reaction and to have an isotope effect of 1. Further, the similarity between the inverse value of the solvent isotope effect for **9a** (k_H/k_D = 4.9) and the solvent isotope effect for **8** (k_H/k_D = 4.1) at 12.5 M methanol also supports the assumption that the C2 radical abstracts hydrogen first, because the formation of both involves hydrogen abstraction by C6 and the formation of one is at the expense of the other. The DNA cleavage efficiency experiments also support this proposal (vide infra).

Table 1: Solvent Isotope Effects on Formation of Drug Products

MeOH (M)	0.25	0.5	1.25	2.5	5.0	12.5
8 (k_D/k_H)	1.8	2.4	2.9	3.0	4.0	4.1
9a (k_H/k_D)	18.0	11.6	9.3	9.1	5.9	4.9
9b (k_H/k_D)	2.3	2.6	1.8	1.9	1.3	1.2

Thus, it is concluded that spirolactone biradical **6** is a relatively stable species; hydrogen abstraction by biradical **6** is slow and sequential, with the C2 radical reacting first and followed by hydrogen abstraction by the more reactive monoradical at C6.

Nucleobases in the DNA Bulge Are not Required for Forming an Effective Bulge Pocket. To further explore the role of the DNA bulge in the formation of cyclospirolactone **8**, the structural requirements for an effective bulge pocket need to be defined. An effective bulge is one that binds the drug efficiently and selectively and can be efficiently cleaved by base-catalyzed activated NCS-chrom. It is possible that every cleavage at a DNA bulge site results in one molecule of cyclospirolactone **8**. Further, it is known that none of the cleavage at a DNA bulge site comes from production of **9**, because cyclospirolactone **8** is the only drug metabolite formed in the presence of excess substrate-bulged DNA, and only **8** contains the hydrogen abstracted from the DNA bulge target nucleotide. In previous papers, point mutations and substitutions of deoxyribonucleotide with ribonucleotide in bulged DNA have revealed certain rules concerning the sequence and structural requirements of an effective bulge (*8*, *9*, *27*−*29*). It has been found that the size of the bulge is important. Base-catalyzed activation of NCS-chrom results in optimal cleavage in bulges of two or three bases, which are also the most effective in formation of **8** (*8*). The

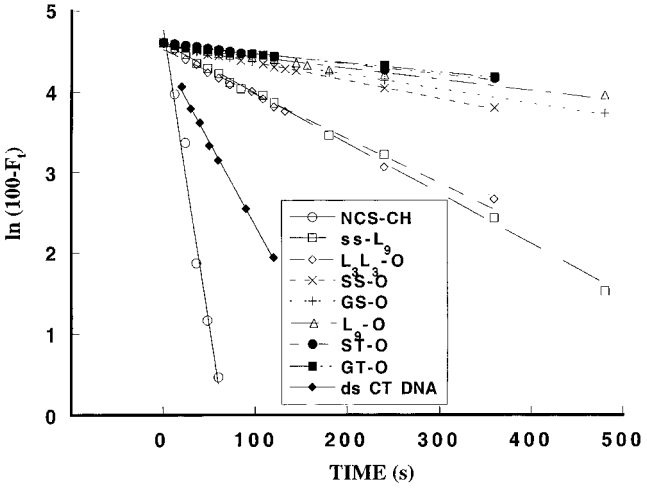

FIGURE 5: Efficiency of different oligonucleotides in the protection of NCS-chrom against degradation. Conditions: 5 μM NCS-chrom in 50 mM Tris·HCl, pH = 8.5, 10% MeOH, either alone (NCS−CH) or with 180 μM (phosphate) calf thymus DNA (ds CT DNA), or in the presence of 2 equiv (10 μM) of oligonucleotide as indicated. Initial rates calculated from the linear equation: $\ln(100 - F_t) = \ln(100 - F_0) - kt$, where F_t is the fluorescence at incubation time t and F_0 is the fluorescence value at $t = 0$. The initial rate constant for the pseudo first-order disappearance of the NCS-chrom is equal to the slope of the line (see Table 2).

substitution of deoxyribonucleotide with ribonucleotide in the bulge leads to some loss of cleavage efficiency and also gives lower production of **8** (*27*). Although the base composition of the bulge has also been found to play some role in the cleavage of the bulge, the precise role of nucleobases in the bulge has not been addressed.

Chemical linker molecules resembling the nucleic acid backbone have been used as substitutes for nonessential nucleotides within a sequence (*30*, *31*). Similarly, 1,2-dideoxyribose has been used to mimic abasic sites in an oligonucleotide (*32*, *33*). It seemed that these moieties might be used as substitutes for the bulged bases in order to study the role of nucleobases in the bulge as NCS-chrom target sites. Thus, different oligonucleotides containing chemical linker molecules, as shown in Figure 1, were synthesized using phosphoramidite chemistry. Bulged structures containing these nucleotide substitutes were based on the double-stranded substrate-bulged oligonucleotide GT-O.

One of the characteristics of the base-catalyzed activation of NCS-chrom is that the inactivation rate of NCS-chrom can be influenced dramatically by the presence of a substrate-bulged DNA and can be easily followed by the fluorescence increase at 550 nm (excitation at 400 nm). The presence of substrate-bulged DNA slows the fluorescence increase substantially (*28*), presumably by providing a tight-binding pocket. This can be used as a simple assay to assess the effectiveness of a particular DNA bulge in complex formation and drug product formation. The initial rate constants of NCS-chrom degradation observed from the fluorescence experiments shown in Figure 5 are summarized in Table 2. It was found that the initial rate constants with oligonucleotide GS-O, ST-O, SS-O, and L_9-O are comparable to those with substrate bulge GT-O, which implies that they act as effective bulges for complex formation. The initial rates of oligonucleotides ss-L_9 and L_3L_3-O are in the middle range between substrate oligonucleotide GT-O and NCS-chrom alone, indicating that these structures, presumably through modified bulge formation or bulges of lower stability, are better than nonbulge containing duplex DNA in protecting against NCS-chrom degradation.

Table 2: Relationships of DNA Binding, DNA Cleavage, and Formation of **8**

code	substrate[a]	$k1$ ($\times 10^{-3}$)[b]	% cleavage[c]	yield of **8** (%)[d]
NCS−CH	NCS−chrom (only)	72.9		≤5
ds CT DNA	calf thymus DNA	20.9		
ss-L_9	5′-CGCAL_9TCGG−3′	6.21	0	≤5
L_3L_3-O	5′-CCGA TGCG-3′ 3′-GGCT ACCG-5′ L_3L_3	5.51	0	≤5
L_9-O	5′-CCGA TGCG-3′ 3′-GGCT ACCG-5′ L_9	1.37	0	≤5
SS-O	5′-CCGATGCG-3′ 3′-GGCTACCG-5′ SS	2.23	0	25
GS-O	5′-CCGATGCG-3′ 3′-GGCTACCG-5′ SG	1.78	≤2	25
ST-O	5′-CCGATGCG-3′ 3′-GGCTACCG-5′ TS	1.25	≤2	36
GT-O	5′-CCGATGCG-3′ 3′-GGCTACCG-5′ TG	1.11	35	56

[a] $L_9 = -(OCH_2CH_2)_3-O-$, $L_3 = -O-(CH_2)_3-O-$; S = 1′,2′-dideoxyribose, as described in Figure 1. [b] $k1$ is the pseudo first rate constant derived from the degradation of NCS−chrom with or without oligomers as described in Figure 5. [c] Percentage of DNA cleavage is from PAGE analysis using PhosporImager as described in Materials and Methods. The reactions contained 50 mM Tris·HCl (pH 8.5), 8 μM oligonucleotide and 11 μM NCS−chrom. [d] Yield of **8** is from HPLC analysis of reaction between oligomer (30 μM) and NCS−chrom (12 μM) in 50 mM Tris·HCl (pH 8.5) buffer incubating for 1 h on ice.

Because these experiments indicate that GS-O, ST-O, SS-O, and L_9-O provide effective bulge binding sites, DNA cleavage experiments were conducted to examine their substrate properties (Figure 6). Interestingly, certain structures that were effective in the protection experiments, such as GS-O, ST-O, SS-O, and L_9-O, were very poorly, if at all, cleaved by NCS-chrom. Piperidine treatment, which expresses abasic site formation or any oxidized backbone, yielded no increase in cleavage. Oligonucleotides ss-L_9 and L_3L_3-O provided poor protection and showed no cleavage. The cleavage of oligonucleotides GS-O and ST-O was site-specific (at the expected 3′-nucleotide in the bulge), although very weak compared to that of GT-O. Quantitation of the DNA cleavage results are summarized in Table 2. The disparity between the two different assays led us to examine the production of cyclospirolactone **8**, because, as shown above, an effective bulge (GT-O) gave **8** in good yield.

Integration of the HPLC peaks corresponding to **8** is summarized in Table 2. Of note is the finding that the poor cleavage substrates GS-O and ST-O gave good yields of **8**; even oligonucleotide SS-O, which gave almost no cleavage, also generated a significant amount of **8**. Oligonucleotides ss-L_9, L_9-O, and L_3L_3-O gave less than 5% yield of **8**. It is interesting that a 20-fold excess of bulged oligonucleotide (100 μM), such as GT-O, GS-O, ST-O, and SS-O, yields the same amount of cyclospirolactone **8**, with no significant other drug metabolites observable (data not shown). These

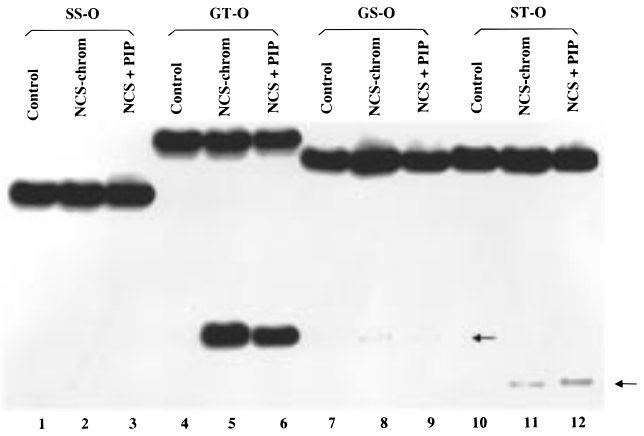

FIGURE 6: Cleavage of different 5′-^{32}P end-labeled bulged oligonucleotides by NCS-chrom. Lanes 1, 2, 3 are with oligonucleotide SS-O; lanes 4, 5, 6 are with oligonucleotide GT-O; lanes 7, 8, 9 are with oligonucleotide GS-O; lanes 10, 11, 12 are with oligonucleotide ST-O; The nomenclature of oligonucleotides is described in Figure 1. Lanes 1, 4, 7, 10 are without NCS-chrom; lanes 2, 5, 8, 11 are with NCS-chrom; lanes 3, 6, 9, 12 are from piperidine treatment after reaction with NCS-chrom. The reactions were carried out by incubating mixtures of 5′-^{32}P end-labeled oligonucleotide (8 μM) and NCS-chrom (11 μM) in 50 mM Tris·HCl (pH 8.5) at 4 °C for 2 h. The mixtures contained 3% methanol.

results show that the bulge pockets formed in GT-O, GS-O, ST-O, and SS-O are effective, with varying efficiency, in accommodating cyclocumulene **5**, the presumptive bulge-binding species. Substitution of 1,2-dideoxyribose (abasic site mimic) for either or both nucleotides at the bulge site presumably generates a bulged structure, which is poorly cleavable but still an effective specific binding site, and efficient in production of **8**.

Thus, nucleobases in the DNA bulge are not required to form an effective bulge pocket. The results in Table 2 show that cleavage of DNA is not stoichiometric with the generation of cyclospirolactone **8**. These three sets of results, protection (binding), strand cleavage, and **8** production, clearly show that while binding of a spirolactone form of the drug to a bulge structure is necessary for **8** formation, not all types of binding are sufficient for generation of the drug product. Further, DNA strand cleavage at the bulge is not essential for **8** formation, although the best substrate GT-O is most efficient in all of these assays. They also show that the stability of the complex comes mainly from stacking interactions of the drug with the helical base pairs above and below the wedge-shaped drug, rather than from the looped-out bases, which ordinarily form the third wall of the triangular prism binding site (*12*). The poor cleavage, coupled with good production of **8**, in reactions between NCS-chrom and oligonucleotides GS-O, ST-O, and SS-O raises the issue of possible turnover by natural bulged DNA in the formation of **8**.

*Observation of Turnover in Production of **8** by DNA Bulge.* When oligonucleotide GT-O was treated with excess NCS-chrom, cyclospirolactone **8** formation exceeded the equivalency of oligonucleotide GT in bulged GT-O (Figure 7). At ratios of drug to bulged DNA of 5 and greater, 3.0−3.5-fold more **8** was produced than there was bulged DNA, assuming all of the GT-containing strand was annealed to the opposite strand. Five-fold excess NCS-chrom resulted in cleavage of essentially all of the bulged oligonucleotide

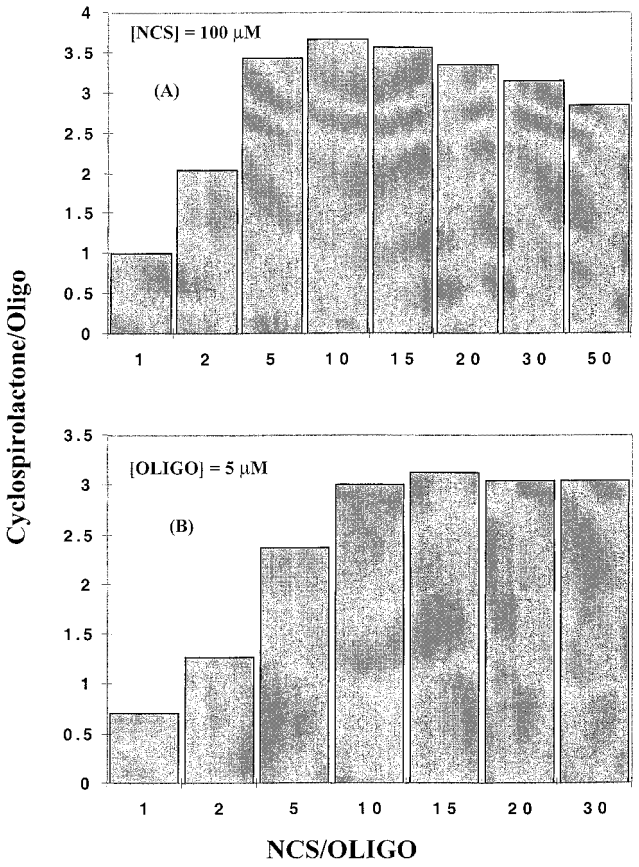

FIGURE 7: Generation of cyclospirolactone **8** per mole of bulged oligonucleotide GT of GT-O in relation to the molar ratio of NCS-chrom to bulged oligonucleotide GT. (A) 100 μM of NCS-chrom and varying concentrations of GT. (B) 5 μM of GT and varying concentrations of NCS-chrom. Quantitation of formation of cyclospirolactone **8** at different ratios of DNA to NCS-chrom was carried out using HPLC as described in Materials and Methods.

GT and gave no cleavage product other than that with a 3′-phosphate, consistent with solely 5′-chemistry.

One can conceive of several possible mechanisms for the generation of at least 3-fold more cyclospirolactone **8** than substrate-bulged oligonucleotide present in the reaction: (1) low cleavage efficiency, resulting in quenching of the C6 radical by solvent; (2) repair of damaged bulged DNA; (3) damaged but not cleaved DNA is still able to form an effective binding bulge for additional drug molecules; and (4) cleaved DNA is still able to form an effective bulge for the formation of **8**. The term cleavage refers to strand-break formation; damage indicates chemical damage on the DNA chain without a strand-break.

The possibility of low cleavage efficiency by NCS-chrom was explored using reactions containing 100 μM of 5′-^{32}P end-labeled oligonucleotide GT of GT-O and 5−100 μM NCS-chrom (Figure 8). Cleavage efficiency of NCS-chrom on bulged oligonucleotide GT was expressed as the percentage of actual cleavage over the theoretical maximal cleavage, where one molecule of NCS-chrom makes one cut at the DNA bulge (Figure 8B). The cleavage efficiency of the reaction was found to be no more than 50%. Thus, at best, only half the drug molecules result in a DNA cut, culminating in a turnover of no higher than 2, leaving open the possibility that additional mechanisms for **8** formation by bulged DNA exist. These results also raise the question as to the basis for

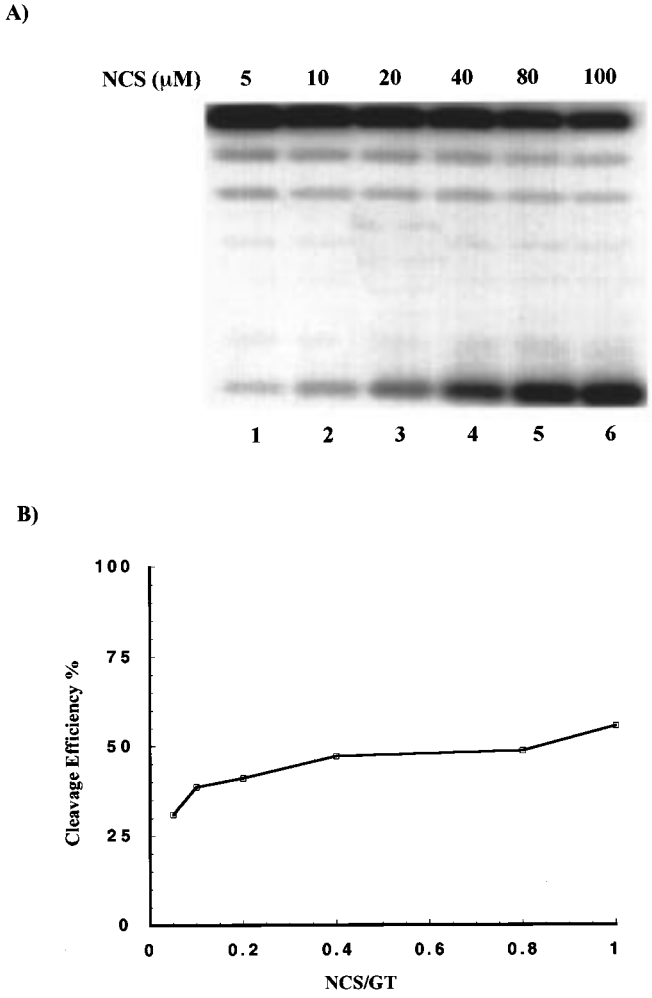

FIGURE 8: Cleavage efficiency of NCS-chrom on bulged oligonucleotide GT of GT-O. (A) PAGE of cleavage reactions performed in a total volume of 40 μL at 4 °C with 50 mM Tris·HCl (pH 8.5) and 100 μM of 5′-^{32}P end-labeled oligonucleotide GT of GT-O. The concentration of NCS-chrom was varied from 5 to 100 μM. Quantitation of PAGE bands was carried out using the PhosphorImager as described in Materials and Methods. (B) Cleavage efficiency is expressed as percentage of actual cleavage over theoretical maximal cleavage, assuming that one molecule of NCS-chrom makes one cut at the DNA bulge.

the low cleavage efficiency. Since cyclospirolactone **8** is the only product found in the reaction with excess bulged DNA, cleavage inefficiency is clearly not due to pathways of drug inactivation other than that leading to **8** formation.

It has been found that spirolactone **9a** binds to DNA bulge site-specifically and tightly ($K_d \sim \mu$M), whereas cyclospirolactone **8** (and **9b**) binds to DNA bulge very poorly, if at all (*29*). It is reasonable to assume that σ,σ-biradical **6** resembles its isostructural form **9a** in its binding to the DNA bulge. If hydrogen abstraction from DNA were carried out by C6 of 2,6-didehydroindacene biradical **6**, it should be a very efficient process, as binding of **6** to the DNA bulge would be strong and its reactivity relatively low; both factors would make for a high efficiency hydrogen abstraction. Accordingly, to account for the relatively low cleavage efficiency would require that the repair of the damaged DNA be efficient. It is unlikely, however, that DNA repair contributes a significant part to the observed 50% cleavage efficiency, because the base-catalyzed cleavage reaction does not involve a thiol reducing agent, and lowering of the concentration of methanol (a major hydrogen source in the reaction) does not improve the cleavage efficiency (unpublished data). On the other hand, if the hydrogen abstraction were carried out by C6 of biradical **7a**, which resembles a monoradical in its reactivity, the DNA hydrogen abstraction process should be less selective and less efficient. Because cyclospirolactone σ,π-biradical **7a** might be expected to more resemble the relatively planar **8** than **6** in its binding at the bulge site, the off-rate of **7a** from the DNA bulge site should be high, and the radical center at C6 might react with solvent, instead of DNA deoxyribose. Actually, because C8″ of **7a** is a sp^3 carbon, **7a** may have a structure that is intermediate between **6** and **8**, with intermediate binding properties. Because C2−C8″ bond formation has already occurred by this stage, the reaction with solvent would still yield cyclospirolactone **8**. The combined result of lower binding of **7a** and more highly reactive C6 in **7a** could account for the observed 50% cleavage efficiency. These data are most consistent with the mechanism proceeding by pathway a, as was also concluded from the results on the solvent isotope effects.

Isolation, Purification, and Identification of 5′-Carboxylic Acid-Ended Oligonucleotide Fragment. Because the relatively low cleavage efficiency cannot account entirely for the observed total turnover of 3, what other factors might contribute to this result? Is it possible that the damaged DNA can still form an effective bulge capable of generating cyclospirolactone **8**? Might even the cleaved DNA form an effective bulge under the influence of the wedge-shaped drug molecule? If a DNA bulge damage intermediate were relatively long-lived and still had the capability to form a stable bulge pocket, then a double oxidation, i.e., sequential single hydrogen abstractions from the target nucleotide deoxyribose by separate molecules of NCS-chrom, might be possible. Thus, a 5′-carboxylic acid-ended oligonucleotide fragment or a 5′-phosphate-ended fragment should be observable (Schemes 3 and 4). As shown in Figure 9, bands with mobilities consistent with the generation of such products are formed and continue to increase with drug dose as the aldehyde product reaches a plateau or actually decreases. To identify the newly formed gel bands, they were excised from the gel, extracted and purified. Chemical and enzymatic methods were then used to identify the isolated samples, as shown in Figure 10. Piperidine treatment of isolated band AL yielded bands CA and PO with disappearance of band AL (lane 4). Reductive treatment of isolated band AL with sodium borohydride or borane gave a new band between bands GT and AL, which has the mobility of the 5′-alcohol (lanes 5 and 6). Treatment of isolated band AL with sodium hypoiodite gave a band, which comigrated with band CA (lane 7), consistent with the oxidation of the 5′-aldehyde to give the 5′-carboxylic acid. These results show that band AL is indeed a 5′-aldehyde-ended fragment and band CA is a 5′-carboxylic acid-ended fragment. As expected, the isolated band CA is resistant to piperidine and calf intestinal phosphatase treatments (lanes 9 and 10). CA band formation has been noted before in thiol-dependent reactions with NCS-chrom (*19*) and calicheamicin (*34*) and duplex DNA, but unlike the reaction described here it does not occur when EDTA is included in the reaction. Presumably, the latter prevents metal-catalyzed autoxidation of the aldehyde. Treatment of isolated band GT with piperidine

Scheme 3: Possible Pathway for Formation of Thymidine 5′-Carboxylic Acid-Ended Fragment

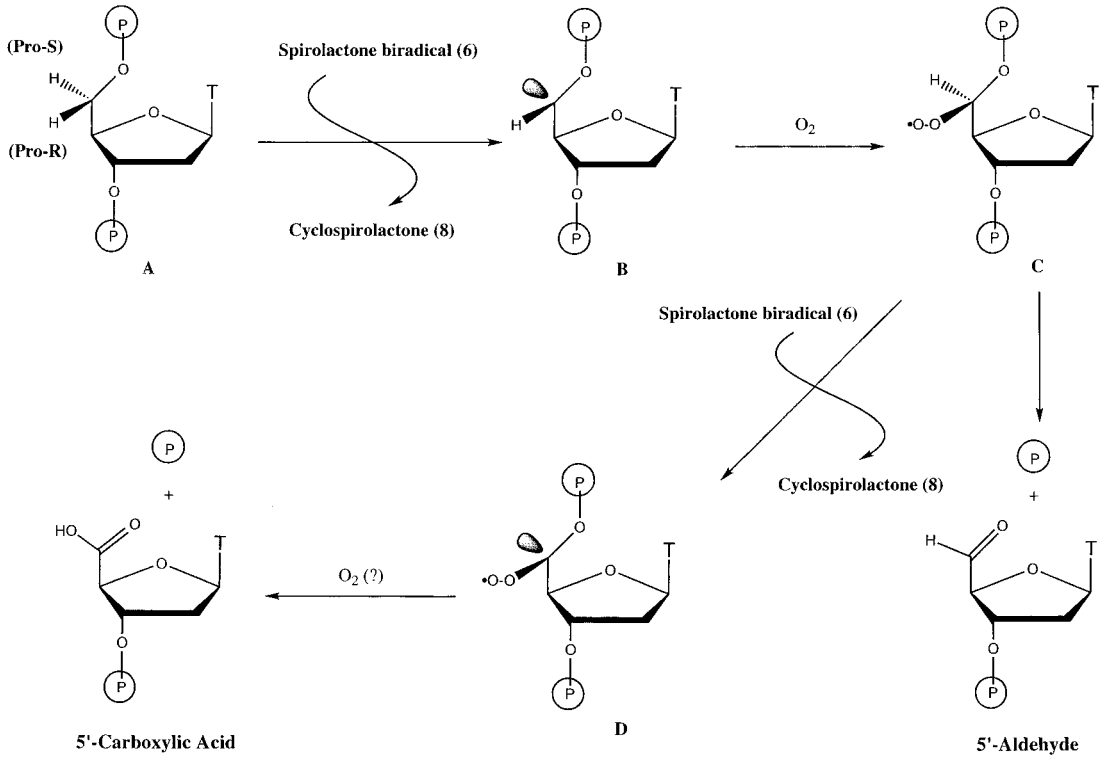

Scheme 4: Possible Pathways for Formation of 5′-Phosphate-Ended Fragment

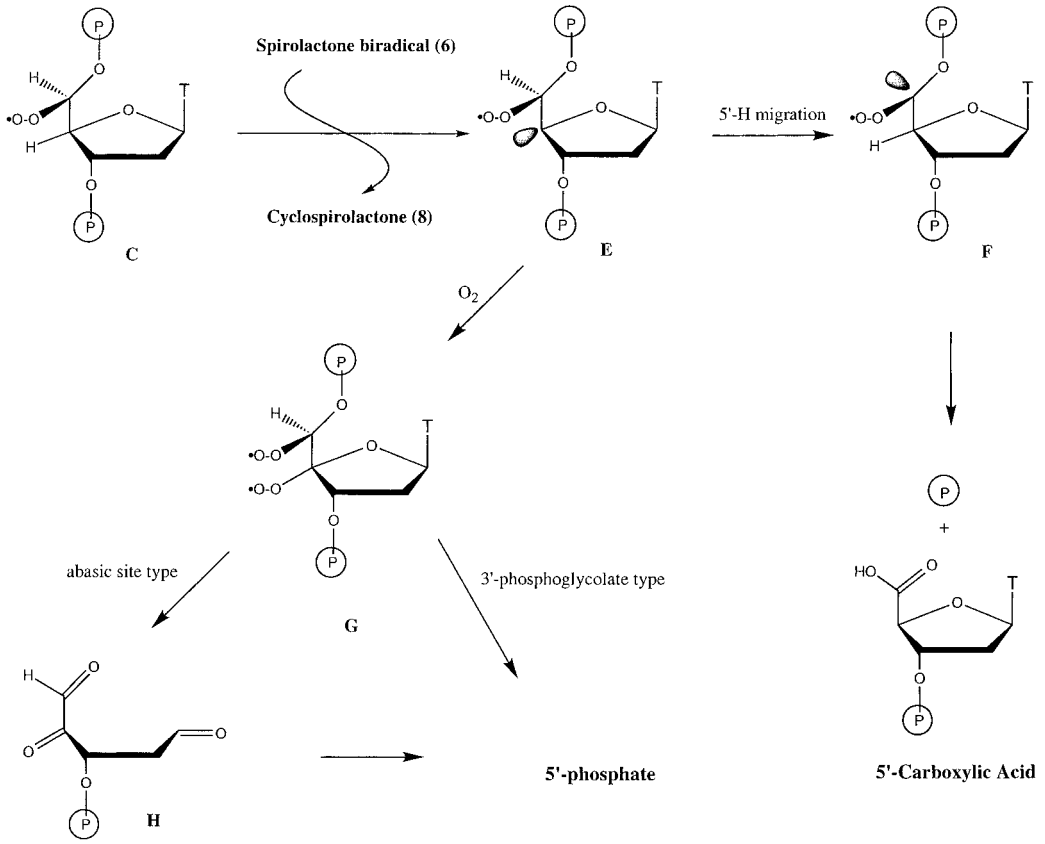

gave no new band (lane 12). Treatment of isolated band PO, the presumed 5′-phosphate-ended fragment, with calf intestinal phosphatase gave a new slow moving 5′-hydroxyl-ended band (lane 14). The isolated band CA was also subjected to HPLC analysis. Enzyme digestion of purified band CA with a mixture of bacterial alkaline phosphatase and snake venom phosphodiesterase gave a nonnatural nucleoside peak, which comigrated with authentic sample of thymidine 5′-carboxylic acid (data not shown). Mass measurement of purified band CA confirmed that it was the thymidine 5′-carboxylic acid-

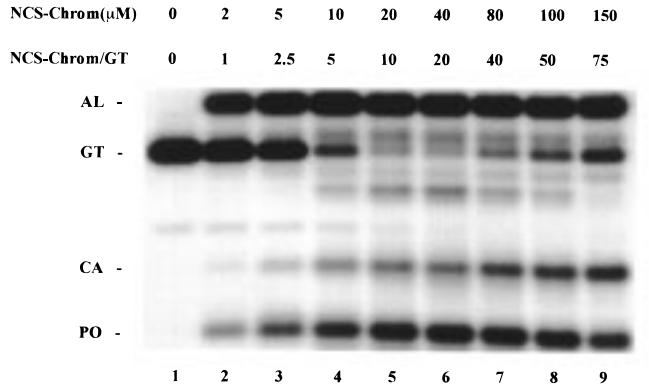

FIGURE 9: Formation of oligonucleotide fragments bearing 5′-carboxylic acid and 5′-phosphate ends. Drug dose response on oligonucleotide fragment formation was assessed using reactions containing 50 mM Tris·HCl (pH 8.5), 2 μM 3′-^{32}P end-labeled oligonucleotide GT of GT-O, and varying concentration of NCS-chrom from 2 to 150 μM on ice for 1 h. Identical results were found whether or not 1 mM EDTA was present. Lane 1, control with no drug; lanes 2−9 with concentration of NCS-chrom at 2, 5, 10, 20, 40, 80, 100, and 150 μM, respectively. AL, GT, CA, and PO denote thymidine 5′-aldehyde-ended oligonucleotide fragment, starting oligonucleotide GT, thymidine 5′-carboxylic acid-ended fragment, and 5′-phosphate-ended fragment band of 5′-pTCG^{32}pG-3′, respectively. The anomously slow mobility of the 5′-aldehyde-ended fragment (slower than the starting oligonucleotide) is characteristic of a short oligonucleotide (*19*). As expected, gels with 5′-^{32}P end-labeled oligonucleotide do not show such a band, ruling out drug adduct formation.

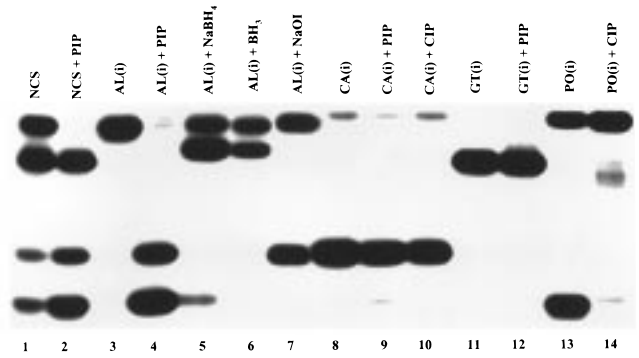

FIGURE 10: Chemical identification of thymidine 5′-carboxylic acid-ended fragment. Lanes 1 and 2, strand cleavage of 2 μM 3′-^{32}P end-labeled oligonucleotide GT of GT-O by 5 μM NCS-chrom before and after piperidine treatment (PIP), respectively; lane 3, isolated thymidine 5′-aldehyde-ended fragment band (AL(i)); lane 4, piperidine treatment of isolated thymidine 5′-aldehyde-ended fragment band; lanes 5 and 6, sodium borohydride or BH_3 treatment of isolated thymidine 5′-aldehyde fragment band, respectively; lane 7, NaOI treatment of AL(i); lanes 8−10, isolated thymidine 5′-carboxylic acid fragment band CA(i), piperidine treatment of CA(i), and calf intestinal phosphatase treatment of CA(i), respectively; lanes 11 and 12, isolated GT band and piperidine treatment of isolated GT band, respectively; lanes 13 and 14, isolated PO band and calf intestinal phosphatase treatment of isolated PO band, respectively. The anomously slow mobility of the hydroxyl-ended fragment produced by CIP treatment is consistent with other reports (*35*). The film was purposely overexposed.

ended fragment 5′-(CA)TTCGG-3′ (CA denotes carboxylic acid, calcd 1507.98, found 1509.56).

The 5′-aldehyde fragment readily eliminates the terminal nucleoside under alkaline conditions, but, to a small extent, also undergoes autoxidation to generate a fragment with a 5′-carboxylic acid end (*19*, *34*). It is conceivable that the observed formation of the 5′-carboxylic acid- and 5′-

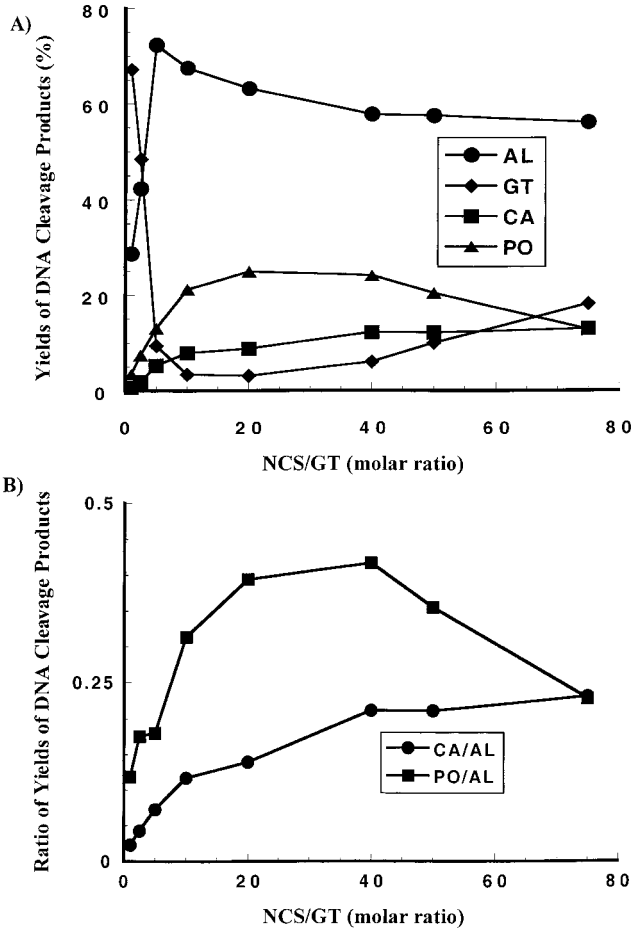

FIGURE 11: (A) Yields of bands CA, PO, GT, and AL versus the molar equivalency of NCS-chrom to GT of GT-O. 100% represents radioactivity in GT at the start of the reaction. (B) Ratios of yields of bands CA, AL, and PO versus the molar equivalency of NCS-chrom to GT of GT-O. Calculations are based on PhosphorImager quantitation of PAGE of Figure 9. CA, AL, PO denote 5′-carboxylic acid-ended fragment band, 5′-aldehyde-ended fragment band, and 5′-phosphate-ended fragment band, respectively, as indicated in Figure 9.

phosphate-ended fragments might, therefore, come from the reaction of the 5′-aldehyde product after the cleavage reaction instead of being caused by sequential oxidations inside the bulge pocket prior to phosphodiester bond cleavage. If the former were true, formation of the 5′-carboxylic acid and 5′-phosphate fragments should be proportional to the formation of the 5′-aldehyde, and they should not be influenced by the molar ratio of NCS-chrom to GT, once aldehyde formation (and cleavage) has reached a maximum. The yields and the ratio of yields of bands CA, AL, and PO were thus plotted against the molar ratio of NCS-chrom to GT (Figure 11). The increasing values of CA/AL and PO/AL vs NCS/GT indicate that bands CA and PO do not come from autoxidation of band AL, but come from the sequential oxidations of the bulge nucleotide target. Consistent with earlier studies (*28*), at very high drug levels, bulge strand cleavage (and 5′-aldehyde- and phosphate-ended fragment formation) actually decreased (Figures 9 and 11).

For the second oxidation to occur, it is required that there be a competent binding pocket at the bulge for the second activated drug molecule. This seems unlikely once the strand break (and 5′-aldehyde terminus) has formed. This was

confirmed by experiments where a second addition of 10−150 μM NCS-chrom for twice the incubation time (2 h) failed to increase the amount of carboxylic acid fragment formed (data not shown). This result also shows that the carboxylic fragment does not result from the direct action of the drug on the aldehyde fragment.

It seems reasonable to propose a mechanism for the formation of the 5′-carboxylic acid derivative (Scheme 3), where the bulge binding pocket for the second activated drug molecule is maintained before the peroxyl radical intermediate species (C) degrades to form a strand break and a 5′-aldehyde-ended fragment. In this mechanism, spirolactone biradical **6** (actually **7a**, vide supra) initially abstracts the *pro-S* hydrogen from the 5′-thymidine residue (A) in the minor groove region of the bulge (*12*). The newly formed 5′-sugar radical (B) is trapped by dioxygen coming from the major groove, which inverses the configuration of the 5′-carbon and converts the remaining hydrogen at the 5′-carbon into a new 5′-*pro-S* hydrogen (C) protruding into the minor groove. Degradation of this damaged DNA results in cleavage and the 5′-aldehyde-ended fragment. If a second spirolactone biradical **6** is bound into the bulge pocket before the strand break, abstraction of the remaining hydrogen at the 5′-carbon will generate a new 5′-carbon radical (D), which could be trapped by a second dioxygen molecule, with subsequent degradation to give a thymidine 5′-carboxylic acid-ended fragment.

To account for the formation of the 5′-phosphate-ended fragment (Figure 9), one can consider three possibilities: (1) spontaneous degradation of the 5′-aldehyde-ended fragment during workup, but the isolated aldehyde-bearing fragment is relatively stable (lane 3, Figure 10); (2) 5′-hydrogen abstraction, followed by oxyradical and subsequent fragmentation to generate a 3′-formyl- and 5′-phosphate-ended fragments, as has been shown to be a minor reaction in the thiol-dependent strand-cleavage reaction (see *1* and references therein); and (3) if the second bound spirolactone biradical **6** abstracts the 4′-hydrogen instead of the 5′-hydrogen, a 5′-phosphate would be formed, and this reaction would contribute to the excess formation of **8**. Possible pathways for the formation of the 5′-phosphate-ended fragment based on (3) are presented in Scheme 4. In this proposal, the second hydrogen abstraction by drug gives a 4′-carbon radical (E). Upon 5′-H migration, a 5′-carbon radical (F) would be formed, which would also lead to the 5′-carboxylic acid derivative. If the 4′-carbon radical (E) is trapped by dioxygen, a diperoxyl radical (G) would result. A phosphoglycolate formation type reaction would lead to the 5′-phosphate (*36*); an abasic site formation type of reaction would also lead to the 5′-phosphate through intermediate (H) (*37*, *38*). Possibility (2) is unlikely, given that 5′-phosphate formation increases at drug levels that do not produce more cleavage.

Although the formation of 5′-carboxylic acid and 5′-phosphate ends constitute minor events, accounting for less than 30% together, their contribution to the observed turnover discussed above can still be significant, assuming that the hydrogen abstraction efficiency by the second drug molecule would be significantly lower than that of the first drug.

Sequential drug-induced oxidative DNA sugar damage leading to a 5′-carboxylic acid-ended fragment has not been previously noted or considered (*39*). It may be that the mechanism leading to its formation in the base-catalyzed DNA bulge reaction is able to occur, not only because the strand-break process is relatively slow and a bulge-like structure is maintained, but because the cleaving species **7a** and its final degradation product **8** bind to the bulged structure less tightly than the biradical **6** (*29*). This allows for a second activated drug molecule to bind to the same bulge site. This situation differs from the thiol-dependent cleavage of duplex DNA by NCS-chrom, where the biradical **3** and its isostructural postactivated form **4** both bind tightly at the target site (*40*).

ACKNOWLEDGMENT

We thank Robert Rieger and Charles Dahl for providing mass measurements. We also thank Lizzy Kappen for a gift of authentic thymidine 5′-carboxylic acid.

REFERENCES

1. Xi, Z., and Goldberg, I. H. (1998) in *Comprehensive Natural Products Chemistry* (Barton, D. H. R., and Nakanishi, K., Eds.) Vol. 7, pp 553-592, Elsevier Science, Oxford.
2. Hensens, O. D., and Goldberg, I. H. (1989) *J. Antibiot. 42*, 761−768.
3. Myers, A. G. (1987) *Tetrahedron Lett. 28*, 4493−4496.
4. Myers, A. G., Proteau, P. J., and Handel, T. M. (1988) *J. Am. Chem. Soc. 110*, 7212−7214.
5. Chin, D. H., Zeng, C.-H., Costello, C. E., and Goldberg, I. H. (1988) *Biochemistry 27*, 8106−8114.
6. Gao, X., Stassinopoulos, A., Rice, J. S., and Goldberg, I. H. (1995) *Biochemistry 34*, 40−49.
7. Kappen, L. S., and Goldberg, I. H. (1993) *Science 261*, 1319−1321.
8. Kappen, L. S., and Goldberg, I. H. (1993) *Biochemistry 32*, 13138−13145.
9. Kappen, L. S., and Goldberg, I. H. (1995) *Biochemistry 34*, 5997−6002.
10. Hensens, O. D., Chin, D. H., Stassinopoulos, A., Zink, D. L., Kappen, L. S., and Goldberg, I. H. (1994) *Proc. Natl. Acad. Sci. U.S.A. 91*, 4534−4538.
11. Hensens, O. D., Helms, G. L., Zink, D. L., Chin, D.-H., Kappen, L. S., and Goldberg, I. H. (1993) *J. Am. Chem. Soc. 115*, 11030−11031.
12. Stassinopoulos, A., Ji, J., Gao, X., and Goldberg, I. H. (1996) *Science 272*, 1943−1946.
13. Cantor, C. R., Warshaw, M. M., and Shapiro H. (1970) *Biopolymers 9*, 1059−1077.
14. Ausubel, F. M., Brent, R., Kingston, R. E., Moore, D. D., Seidman, G. G., Smith, J. A., and Struhl, K. (1989) *Current Protocols in Molecular Biology*, John Wiley and Sons, New York.
15. Myers, A. G., Cohen, S. B., and Kwon, B. M. (1994) *J. Am. Chem. Soc. 116*, 1255−1271.
16. Chin, D. H., Kappen, L. S., and Goldberg, I. H. (1987) *Proc. Natl. Acad. Sci. U.S.A. 84*, 7070−7074.
17. Kappen, L. S., and Goldberg, I. H. (1992) *Biochemistry 31*, 9081−9089.
18. Kappen, L. S., and Goldberg, I. H. (1997) *Biochemistry 36*, 14861−14867.
19. Kappen, L. S., and Goldberg, I. H. (1983) *Biochemistry 22*, 4872−4878.
20. Dedon, P. C., and Goldberg, I. H. (1992) *Biochemistry 31*, 1909−1917.
21. Chen, P. (1996) *Angew. Chem., Int. Ed. Engl. 35*, 1478−1480.
22. Logan, C. F., and Chen, P. (1996) *J. Am. Chem. Soc. 118*, 2113-2114.
23. Schottelius, M. J., and Chen, P. (1996) *J. Am. Chem. Soc. 118*, 4896−4903.
24. Yoshida, K.-I., Minami, Y., Otani, T., Tada, Y., and Hirama, M. (1994) *Tetrahedron Lett. 35*, 5253−5256.
25. Iida, K., and Hirama, M. (1995) *J. Am. Chem. Soc. 117*, 8875−8876.

26. Curran, D. P. (1988) *Synthesis*, 417−439, 489−513.
27. Kappen, L. S., Xi, Z., and Goldberg, I. H. (1997) *Bioorg. Med. Chem. 5*, 1221−1227.
28. Stassinopoulos, A., and Goldberg, I. H. (1995) *Biochemistry 34*, 15359−15374.
29. Yang, C. F., Stassinopoulos, A., and Goldberg, I. H. (1995) *Biochemistry 34*, 2267−2275.
30. Durand, M., Chevrie, K., Chassignol, M., Thuong, N. T., and Maurizot, J. C. (1990) *Nucleic Acids Res. 18*, 6353.
31. Salunkhe, M., Wu, T. F., and Letsinger, R. L. (1992) *J. Am. Chem. Soc. 114*, 8768−8772.
32. Takeshita, M., Chang, C. N., Johnson, F., Will, S., and Grollman, A. P. (1987) *J. Biol. Chem. 262*, 10171−10179.
33. Kalnik, M. W., Chang, C. N., Grollman, A. P., and Patel, D. J. (1988) *Biochemistry 27*, 924−931.
34. Zein, N., Sinha, A. M., McGahren, W. J., and Ellestad, G. A. (1988) *Science 240*, 1198−1201.
35. Mohanty, U., Searls, T., and McLaughlin, L. W. (1998) *J. Am. Chem. Soc. 120*, 8275−8276.
36. Kappen, L. S., Goldberg, I. H., Frank, B. L., Worth, L., Jr., Christner, D. F., Kozarich, J. W., and Stubbe, J. (1991) *Biochemistry 30*, 2034−2042.
37. Frank, B. L., Worth, L., Jr., Christner, D. F., Kozarich, J. W., Stubbe, J., Kappen, L. S., and Goldberg, I. H. (1991) *J. Am. Chem. Soc. 113*, 2271−2275.
38. Saito, I., Kawabata, H., Fujiwara, T., Sugiyama, H., and Matsuura, T. (1989) *J. Am. Chem. Soc. 111*, 8302−8303.
39. Pogozelski, W. K., and Tullius, T. D. (1998) *Chem. Rev. 98*, 1089−1107.
40. Stassinopoulos, A., and Goldberg, I. H. (1995) *Bioorg. Med. Chem. 3*, 713−721.

BI982734I